Precision agriculture for sustainability

Second edition

Edited by Dr John Stafford, Silsoe Solutions, UK

E-CHAPTER FROM THIS BOOK



Developments in proximal crop sensing for precision agriculture

Mats Söderström, Bruno Morandin Figueiredo, Lena Engström, Omran Alshihabi, Kristin Persson, Swedish University of Agricultural Sciences (SLU), Sweden

- 1 Introduction
- 2 Precision agriculture for sustainable crop production
- 3 The electromagnetic spectrum reflection characteristics of light from a crop
- 4 Site-specific weed management and variable-rate application of nitrogen with proximal sensors
- 5 Examples of handheld sensors and sensors in contact with plants
- 6 Case Study 1: Comparison of sensors for prediction of N uptake in oats
- 7 Case Study 2: Evaluation and upscaling of portable tools for crude protein determination and field mapping in conjunction with Sentinel-2 satellite imagery
- 8 Outlook and Conclusion
- 9 Where to look for further information
- 10 References

1 Introduction

1.1 What is proximal crop sensing?

Proximal sensing refers to measurements using sensors in close proximity to the object of interest (Adamchuk et al. 2018). Proximal crop sensors are used to collect information about a growing crop and can be mounted on the ground, handheld or borne by vehicles such as tractors or robots. Remote sensing involves the measurement of crop properties often with similar equipment as used in proximal sensing, but from a greater distance, using satellites, airplanes or unmanned aerial vehicles (UAVs, drones). The latter may also be used at short distances. At the other end of the spatial scale, there are sensors that can be used very close to, or in contact with, plant parts. Hence, there is a wide range of different types of sensors and scales on which they are used. Different

Cambridge, UK, 2025, (ISBN: 978 1 80146 881 7; www.bdspublishing.com)

sensors can also be used in combination, e.g. a proximal sensor can be used to calibrate data collected by remote sensing (Fig. 1).

In most cases, crop sensors collect inferential data, i.e. they do not directly measure crop properties of interest but rather produce a metric that can be used to estimate these properties. For example, light in different wavelengths reflected by a crop canopy can be recorded by a crop sensor and translated into useful information for agricultural management using established empirical relationships with e.g. the protein content of the crop.

Proximal crop sensors are used to assess and predict a range of different crop conditions, such as nutrient status, incidence of weeds and diseases, and drought stress in plants. The ripening stage of fruits and even number of spikes in a wheat stand can also be determined from digital images. Rapid technological development and access to artificial intelligence and machine learning methods have enabled new applications that were not possible just a few years ago, while still employing sensor techniques that have been used for a number of years.

1.2 Aim of this chapter

This chapter presents an overview of proximal sensing techniques used in practical precision agriculture, with the overall aim of contributing to more sustainable crop production. To provide perspective on the usefulness of crop sensors, the chapter starts with an example of why site-specific crop management is important and how it relates to sustainable production. The basics of crop canopy reflectance are then presented, followed by an

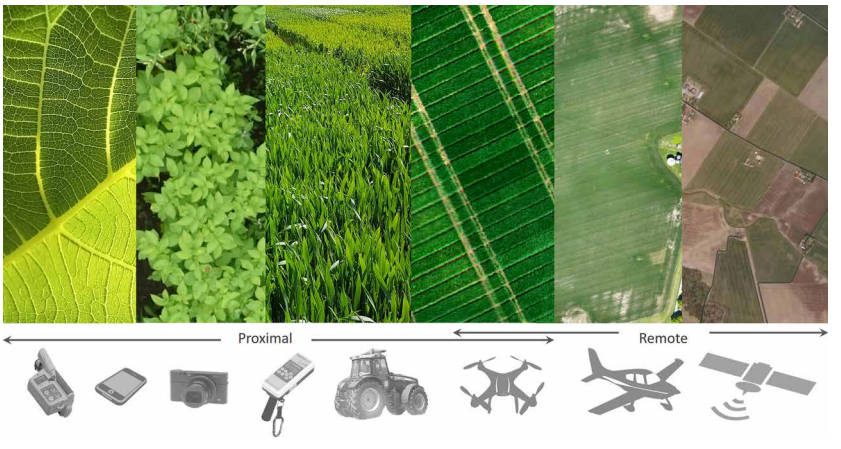


Figure 1 Crop sensors used in precision agriculture may cover a range of spatial scales, from individual leaf to landscape. Sensors used within a few metres of the crop canopy are called proximal sensors. Drones can be used for proximal sensing or remote sensing.

introduction to two practical precision agriculture techniques, site-specific weed management and real-time crop sensing, mainly focusing on within-field nitrogen application. Two case studies in which different types of proximal sensors are used, individually or in combination with other techniques (UAVs and satellites), are described. Finally, potential future developments are briefly discussed.

2 Precision agriculture for sustainable crop production

2.1 What is sustainable crop production?

Sustainable crop production refers to the practice of growing crops in a way that minimises negative impacts on the environment, while also ensuring long-term productivity and economic viability. It involves using methods and techniques that promote soil health, conserve water, protect biodiversity and optimise the use of inputs such as pesticides and fertilisers. Sustainable crop production aims to meet the current needs of food production without compromising the ability of future generations to meet their own needs (Brodt et al. 2011). Since the global cropland area is finite, methods are needed to achieve sustainable intensification (European Parliament 2019). Precision agriculture is one approach often promoted to achieve more sustainable crop production.

In precision agriculture, whether organic or conventional, the goal is often to apply optimum rates of various inputs, e.g. fertilisers (see the definition of precision agriculture on the website of the International Society of Precision Agriculture: www.ispag.org). More specifically, the target is often economic optimisation, i.e. not the input rates that give the highest yields, but those that provide the optimum balance between input costs, desired yield quality, grain price etc. The need to avoid nutrient losses to the atmosphere or through leaching or erosion adds additional complexity, making it difficult to identify the economic optimum in practice. During the cropping season, when fertilisers need to be applied, crucial information is lacking on e.g. the amount of rainfall during coming months and the amount of nutrients that will be supplied from the soil.

2.2 Economic optimisation with crop sensors - an example of spatial variation in a wheat field

An example of how the economic optimum nitrogen (N) rate (EONR) can vary within part of a wheat (*Triticum aestivum* L.) field is shown in Fig. 2. It is evident that a uniform N rate for the entire field is not appropriate (Fig. 2a). In the example, average EONR is 154 kg N ha⁻¹ (range 82-225 kg N ha⁻¹). The average yield at this EONR (Fig. 2b) is $8.34 \, \text{t} \, \text{ha}^{-1}$ (range $5.1-10.5 \, \text{t} \, \text{ha}^{-1}$), with an average protein content of 11.7% (range 10.6-13.7%) (Fig. 2c). In this example,

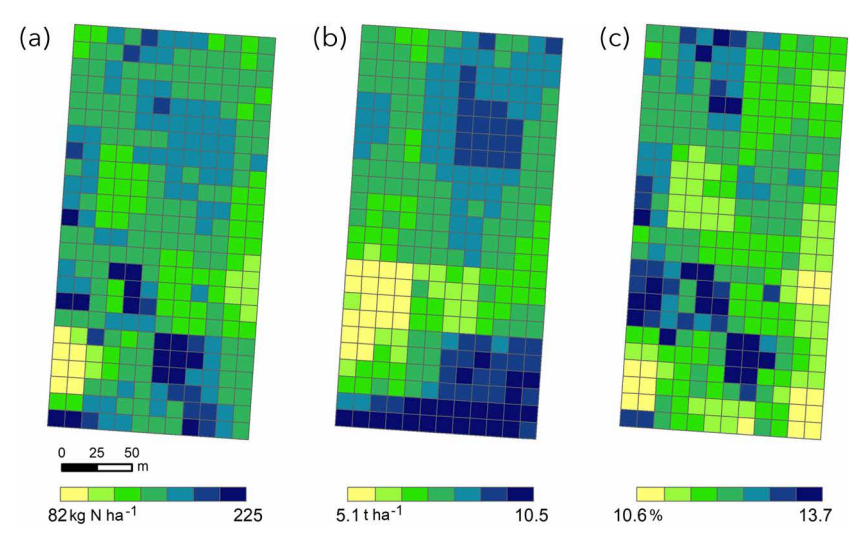


Figure 2 Example of spatial variation in an approximately 3 ha area of a winter wheat field in Sweden, where each cell is $12 \text{ m} \times 12 \text{ m}$: (a) Economic optimum nitrogen rate (EONR), (b) grain yield at EONR and (c) grain protein content at EONR.

the N response curves of grain yield and protein concentration, and thereby EONR, are known for every single $12 \text{ m} \times 12 \text{ m}$ grid cell of the area (through a so-called chessboard trial, the principle of which is described in e.g. Kindred et al. (2016)). In a real situation, this is never the case. At best, the field-average N requirement is predicted early in the cropping season based on an estimate of future yield combined with an estimate of N supply from the soil. To better account for crop growing conditions during the season, the total N dose can be split into a few split applications (2–4) over time. Use of crop sensors to assess crop growth and N uptake before every split application can be one way to optimise the N requirement in different parts of a field.

3 The electromagnetic spectrum - reflection characteristics of light from a crop

Light falling onto a plant leaf is either reflected from the leaf surface, absorbed or transmitted through the leaf. Most crop sensors used in precision agriculture measure the reflectance of light or transmittance through the leaf. These sensors may be used *in situ*, in contact with the object (e.g. leaf, stem or ear) or at a distance from the crop (e.g. mounted on a tractor or carried by hand). Some sensors have their own light source (active sensors), whereas others rely on incoming sunlight (passive sensors).

A growing crop may reflect light as shown in Fig. 3. The reflectance characteristics of a crop are called its spectral signature. Different types of crops

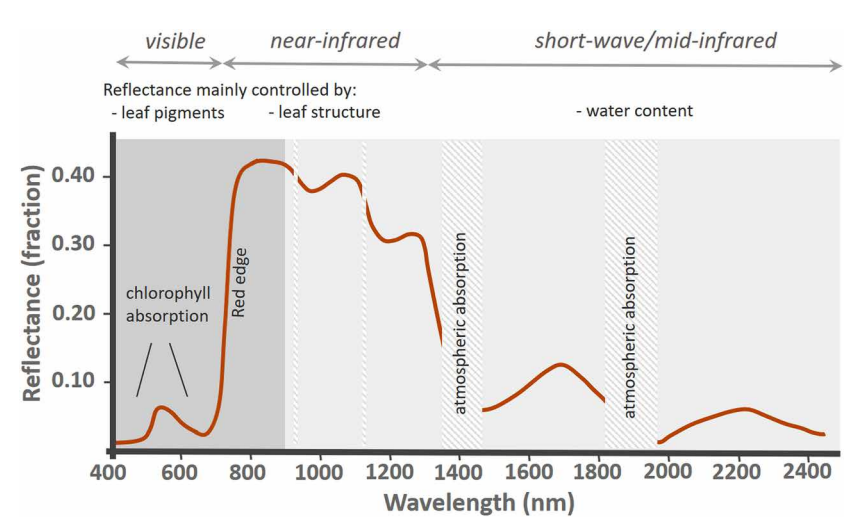


Figure 3 Generalised spectral signature (reflectance) of a cereal crop canopy in the visible to short-wave infrared region of the electromagnetic spectrum, which is commonly used in remote sensing. Most proximal crop sensors currently used in precision agriculture record light in the visible to near-infrared region. Reflectance refers to the reflected fraction of incoming light.

or even different cultivars of the same crop may have their own spectral signature, with slight shifts from the curve shown in Fig. 3. This shift is used e.g. in crop type classification with satellite image analysis. Green, healthy vegetation reflects only a small amount of the incoming visible light, in the photosynthetically active radiation spectral region (400-700 nm). Leaf chlorophyll absorbs especially blue and red light, which is used as a source of energy for photosynthesis, while somewhat more of the green light in solar radiation is reflected. At slightly longer wavelengths (>700 nm), much more light is reflected, with a sharp increase in reflectance up to around 780 nm (Fig. 3). This part of the spectrum is referred to as the red edge and is part of the near-infrared region (NIR) in which the cell structure of the leaves reflects about half of all incoming light. In the short-wave infrared (SWIR) region (sometimes also called the mid-infrared region, MIR), from 1300 to 2500 nm, reflectance is lower due to absorption related to plant water content (lower water content results in higher reflectance). Some of the satellites used in precision agriculture (e.g. Landsat and Sentinel-2) record light also in the SWIR region, but it is less common for proximal sensors currently used in practical precision agriculture to have the ability to measure reflectance in this part of the spectrum. The thermal infrared region (TIR) refers to longwave infrared light, commonly encompassing wavelengths between 8000 and 14 000 nm (beyond the scale in Fig. 3) and is of interest in measurements with thermal sensors. All objects with temperature above 0 K, including vegetation, emit heat in the form of long-wave energy.

The dramatic differences in light reflectance in the visible to NIR part of the spectrum are of particular importance in crop sensing in precision agriculture (Fig. 4). Many crop sensors use the difference in reflectance between the NIR region and the visible region of the electromagnetic spectrum to deliver information on crop status. As can be seen in Fig. 4, the spectral signature of a wheat crop varies in a typical manner according to the amount of N applied, provided that N is the limiting factor for crop growth. Wheat receiving 0 kg N ha⁻¹ displays high reflectance in the visible wavebands and lower reflectance in the NIR region. An increasing amount of N lowers the reflectance in the visible bands and increases the reflectance in the NIR bands, in the case shown with a large increase when 80 kg N is added and a smaller increase when successively higher N dose is used until at some level there is no increase. In principle, this interaction between reflectance and N is the basis for the use of crop sensors in precision agriculture.

Figure 4 shows the wavebands of different types of crop sensors, with different symbols indicating the bandwidth. These are satellites Sentinel-2

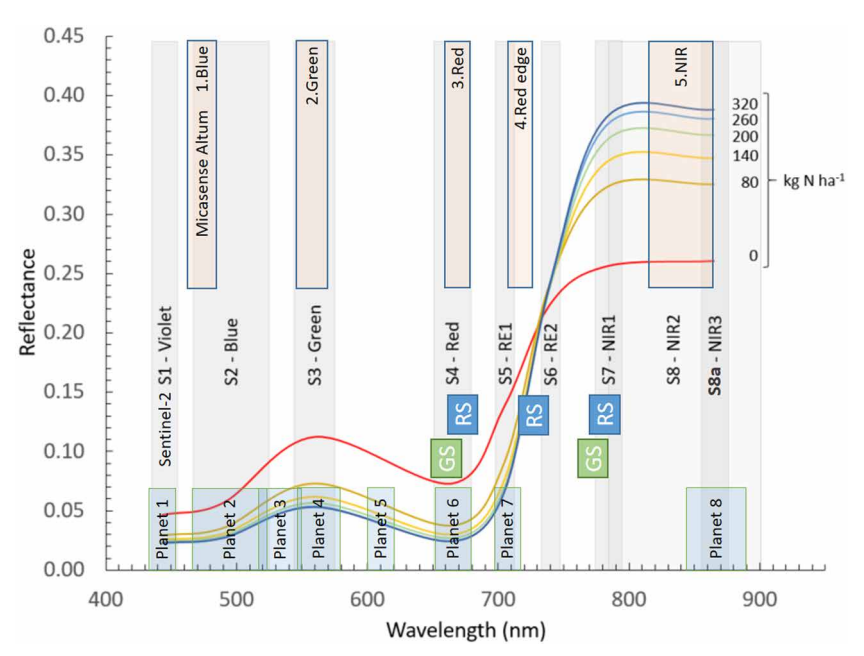


Figure 4 Crop canopy reflectance of a winter wheat crop (cv. Julius) just after flowering (Zadoks growth stage DC 69-75; Zadoks et al. 1973). Data from 10 Swedish field trials 2019–2021 testing six nitrogen (N) rates (described in Piikki et al. 2022). Band recordings by different sensor types are shown with different symbols: Satellites: Sentinel-2 (ESA, France) and Planetscope (Planet, USA); drone camera: Micasense Altum (AgEagle, USA); handheld: GreenSeeker, GS (Trimble/Case, USA), RapidScan CS-45, RS (Holland Scientific, USA).

(ESA, France) and Planetscope (Planet, USA), the Micasense Altum (AgEagle, USA) drone camera, and the handheld proximal sensors GreenSeeker (Trimble/ Case, USA) and RapidScan CS-45 (Holland Scientific, USA). Optical satellite sensors and optical drone sensors are passive sensors, whereas the handheld GreenSeeker and RapidScan sensors have their own light source. The bands available can be used to describe the difference in reflectance between the visible and NIR regions. This is most often done by combining reflectance (ρ) data from two or more bands into a vegetation index, commonly a normalised difference index (NDI) where: $NDI_{i,j} = ([\rho_i - \rho_j]/[\rho_i + \rho_j])$. Examples are normalised difference vegetation index (NDVI) and normalised difference red edge index (NDRE):

$$NDVI = (\rho_{NIR} - \rho_{Red})/(\rho_{NIR} + \rho_{Red})$$
 (Eq. 1)

$$NDRE = (\rho_{NIR} - \rho_{Red \, edge})/(\rho_{NIR} + \rho_{Red \, edge})$$
 (Eq. 2)

As can be seen in Fig. 4, the bands recorded by different sensors are slightly different in terms of wavelengths and bandwidths. This means that indices such as NDVI and NDRE differ somewhat between sensors.

There are hundreds of different indices described in the literature (see e.g. the on-line Index Database: https://www.indexdatabase.de/), often with the aim of finding band combinations that are empirically well related to various crop properties. The challenge is that different stresses affecting the crop may be difficult to distinguish using reflectance in a few wavebands. In general, more and narrower bands make it possible to describe the spectral characteristics of a crop more precisely. A multispectral sensor is able to record reflectance in several bands. A sensor with a large number of bands over a continuous spectral range is called a hyperspectral sensor. Such sensors may have several hundred bands and are used in research but are not commonly used in practical precision agriculture.

4 Site-specific weed management and variable-rate application of nitrogen with proximal sensors

Two main uses of proximal crop sensors are in site-specific weed management (SSWM) and variable-rate application of N. In SSWM, this often involves using cameras mounted on a spray boom to detect visible light (red-green-blue, RGB) at very high spatial resolution to allow for feature detection to separate weeds and crops. In variable-rate N application, it is more common to use spectrometers detecting reflectance from the crop canopy in different wavelengths in the visible to NIR region of the electromagnetic spectrum. Typically, these applications of proximal crop sensors take place at certain times of the growing season. Figure 5 indicates the two periods during which SSWM and variable-rate N application

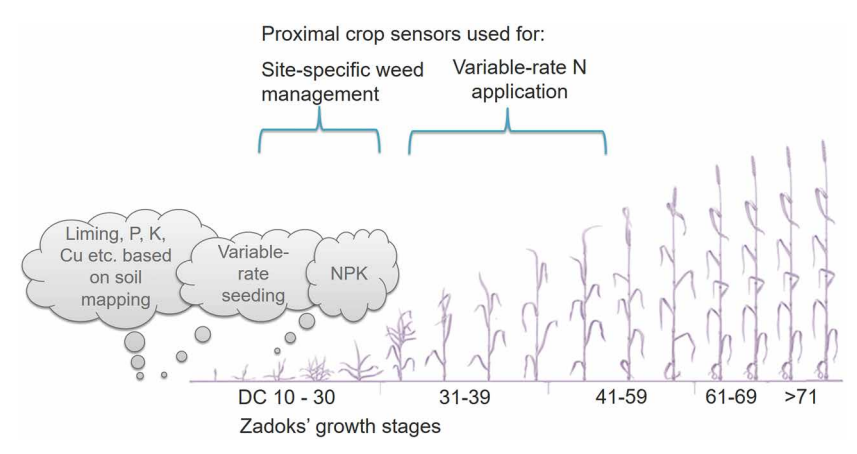


Figure 5 Examples of timing of different management actions in a growing cereal crop. Site-specific weed management using proximal cameras takes place early in the crop season. Variable-rate nitrogen (N) application is typically undertaken during stem elongation. Liming and phosphorus and potassium fertilisation are normally carried out before the season.

are undertaken in cereals, the example is wheat in Scandinavia. Weed scanning is done before the crop becomes too dense, possibly until the beginning of stem elongation (stage DC 30), whereas variable-rate N application based on crop sensing is commonly carried out during stem elongation to booting. For fertilisation, this is typically in split-dose application strategies, where a first dose of N (or NPK) may be applied at a uniform rate and subsequent doses are based on crop status, to adapt to within-field variability and varying mineralisation of soil N, which can be caused by seasonal rainfall and temperature patterns.

In the management approach depicted in Fig. 5, application of other major nutrients, such as phosphorus and potassium, and adjustment of soil pH with lime are carried out before the cropping season, based on soil mapping (and/or with proximal soil sensors if precision agriculture practices are employed). The seed rate may also be varied based on e.g. soil texture conditions. As mentioned, a first uniform N dose is applied early in the season (further details on precision soil management are provided in other chapters of this book). Since it is challenging to predict N requirement before the cropping season, it can be advantageous to add N on a few occasions during the season in order to come as close as possible to the EONR (see Fig. 2). Targeting the optimal N rate is beneficial for the quantity and quality of yield but also for reducing losses of N through leaching and volatilisation (Karlsson Potter et al. 2022). There is a considerable potential to increase the N use efficiency in agriculture, which on a global scale is estimated to be only 33% (Raun and Johnson 1999).

4.1 Crop sensors for site-specific weed management

The goal of SSWM can be to reduce the use of herbicides in conventional farming or to control weeds mechanically. Camera-guided inter-row hoeing is of interest in both organic and conventional farming and allows for precise tracking of crop rows and adjustment of the implement (Gerhards *et al.* 2022). Chemical weed management in precision agriculture based on crop sensors mainly consists of three parts: (1) recognition and mapping of weeds, (2) assessment of suitable treatment and (3) actual weeding, e.g. on-or-off spraying. Weeds commonly occur non-uniformly in a field, often in patches. Avoiding a flat rate can therefore often reduce herbicide use substantially, by 50–90% (Gerhards *et al.* 2022). This can contribute substantially to overall environmental policy goals such as the European Union Green Deal to reduce chemical use and increase biodiversity (European Parliament 2019).

Systems for weeding can be off-line or real-time. In an off-line system, mapping of weed occurrence is carried out beforehand, e.g. using drones or cameras mounted on a vehicle (Rasmussen et al. 2013). In a real-time system, a number of cameras can instead be mounted on a spray boom, allowing instant image analysis of weed occurrence, and the outcome immediately controls the spraying pattern. The off-line approach has the advantage that the user can see the results of mapping for the whole field in advance and take decisions on treatment in a more interactive manner, e.g. it is possible to determine the exact amount of herbicides needed. The real-time approach requires less time and can be entirely automated. The process of distinguishing weeds from crops with image analysis is a major challenge and there is a considerable amount of research dealing with this matter (see reviews by e.g. Allmendinger et al. 2022; Gerhards et al. 2022; Hu et al. 2024). The most straightforward situation is when weeds are the only green vegetation present, e.g. colonising bare soil after harvest of a grain crop ("green-on-brown"). A simple green-red vegetation index or an index based on visible and near-infrared wavebands works well for weed mapping in this case. It is more complicated to automatically distinguish weeds in a growing green crop ('green-on-green'). The most challenging task is separating grassy weeds in a cereal crop, while broadleaf weeds are easier to recognise.

Major manufacturers of agricultural services offer solutions for camera-controlled chemical spraying, such as the John Deere See & Spray Select system and the Bosch/BASF One Smart Spray system. A challenge in this regard is the lack of standard protocols for linking detection and weed treatment systems (Gerhards et al. 2022). Some commercially available systems, such as the WeedSeeker and Bilberry SSWM (by Trimble/AGCO) and the DAT Ecopatch (Dimensions Agri Technologies, AS, Norway), can be mounted directly on an existing sprayer if it is equipped with the ISOBUS communication system. The



Figure 6 Cameras for weed detection, mounted on a spray boom. Images are taken continuously and analysed for weed and crop coverage in real time. Inset: original image (left) and classified image (right). Source: Photo adapted from: Dimensions Agri Technologies, Norway.

DAT Ecopatch system consists of downward-looking RGB cameras (as opposed to forward-looking cameras in some other systems) that are placed 3-4 m apart along the boom (Fig. 6). As with other similar systems, image analysis is done with a machine learning/artificial intelligence algorithm that predicts green-ongreen weed coverage and crop coverage, most efficiently up to the growth stage around DC 30 (as indicated in Fig. 5). The DAT system uses a patch spraying approach, which means that an entire section of the sprayer is on-or-off depending on the image analysis results, and patches or groups of weeds are sprayed – an approach that is proven suitable in small-grain cereals. An alternative is systems that aim for spot spraying, which can target even single plants (Allmedinger et al. 2022).

4.2 Tractor-mounted crop sensors for real-time management

Tractor-mounted sensors are among the most widely used tools in practical precision agriculture. They are mainly used not only in small-grain cereals and maize but also in e.g. potato and oilseed rape. They are based on the principle that a tractor-mounted crop sensor (typically on the cab roof or a front-boom) scans the crop canopy, most commonly for applying variable-rate N according to crop status. Sensed signals of crop canopy reflectance in different wavebands are directly processed in the tractor, and a calibration model computes a suitable amount of N to apply (Fig. 7). This information is then sent via some form of application rate controller that adjusts the spreader accordingly. The sensors used in real-time scanning can be active or passive.

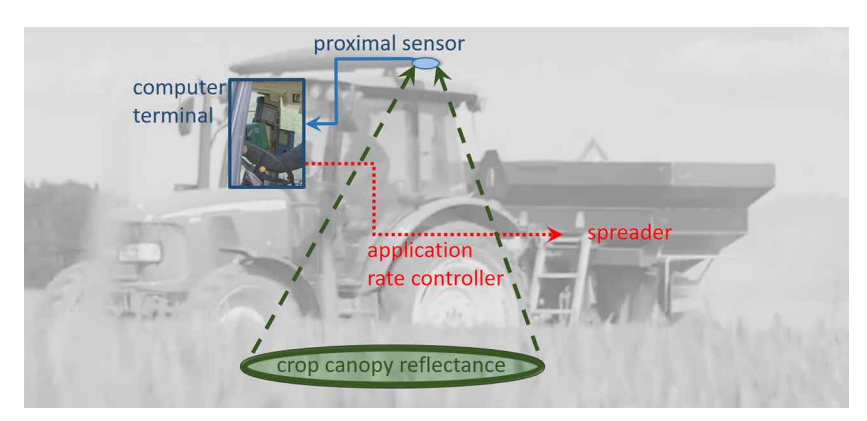


Figure 7 Schematic view of a tractor-mounted proximal crop sensor used for real-time variable-rate application of fertiliser (most commonly nitrogen).

In addition to N management, these systems are e.g. also used for variable fungicide application, adapting the rate according to biomass variation.

An example of a passive sensor is the first version of the Yara N-Sensor (Yara, Norway), which was introduced commercially in the late 1990s (Heege 2013). To handle differences in ambient light, that sensor simultaneously recorded incident light through an upward pointing sensor to correct for varying light levels, while one spectrometer registered reflectance in four spots around the vehicle (two on each side) at an angle of around 60°. This was originally a hyperspectral sensor with 45 bands in the range 450–900 nm (10 nm wide) but only two bands in the red edge region were used to estimate an internal vegetation index (Reusch 2006). An assessment of how different band combinations is related to N uptake in winter wheat was done by Reusch (2005). Wolters et al (2021) showed that a chlorophyll index (using the bands 740 nm and 783 nm) calculated by Sentinel-2 satellite images can predict very similar within-field maps of N uptake as those obtained with a tractor-borne Yara N-Sensor (mean absolute difference 7 kg N ha⁻¹ on comparing data from 13 wheat fields).

It is more common today to use active sensors in real-time scanning and application. By using light-emitting diodes or laser diodes the sensors become independent of sunlight, so scanning can be done at night or with varying cloud cover. Examples of active commercial on-the-go instruments for crop sensing are GreenSeeker (Trimble/Case, USA) (using two bands calculating NDVI (red 660 nm, NIR 770 nm; see Fig. 4)), OptRx sensor (AgLeader, USA) (using three bands, 670, 730 and 780 nm; same as RapidScan shown in Fig. 4) and CropSpec (TopCon, Japan) (two bands, 735 and 805 nm). The active version of the Yara N-Sensor, ALS, records reflectance in the bands 730, 760, 900, 970 nm (Reusch 2006), while its successor, ALS-2, uses four bands in the red-to-red edge region

and a xenon flashlamp as light source. ISARIA (Fritzmeier, Germany) is another active sensor solution, with proprietary indices depicting biomass and N status.

An essential component of these real-time systems is an agronomic model for converting the reflectance data obtained into management information, such as an N rate to apply. In Fig. 8, this model is exemplified as a grey central box, between sensor maps on top and variable-rate N maps below. The rectangular pattern ($12 \text{ m} \times 24 \text{ m}$ along tramlines) in the N rate maps in Fig. 8 coincides with the 24-m wide boom spreader used by this farmer. The tractor sensor used by the farmer is a Yara N-Sensor ALS and the N topdressing map shown is output from the model used by that system. The other two N rate maps are simply based on correlation between the N-Sensor and the other sensors (coefficient of determination R^2 in this case between data from the tractor index

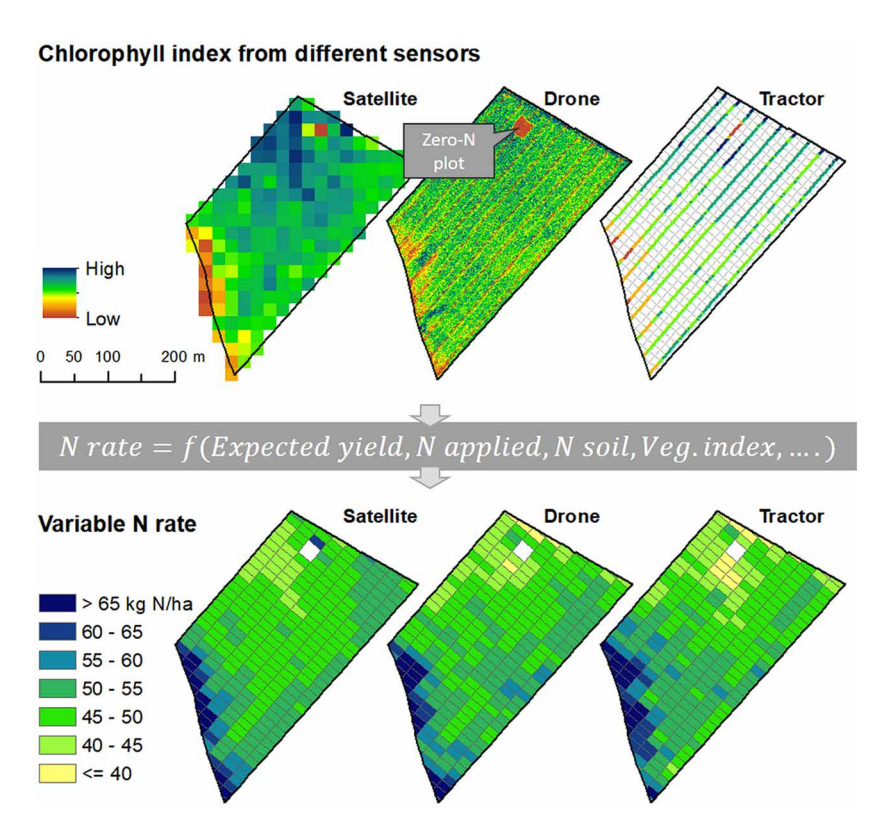


Figure 8 Upper panels: Maps of chlorophyll index from different sensors in a 7.7-ha wheat field in south-west Sweden at late stem elongation (DC 39; time of supplementary N fertilisation). The grey box represents an agronomic model. Lower panels: N application maps based on different sensors (tractor sensor Yara N-Sensor ALS, satellite image Sentinel-2 (20-m pixels), drone camera Micasense Altum; all data collected within five days). The zero-N plot received no N previously during the season. Diagram modified from Nilsson et al. (2023).

and the drone camera and satellite is 0.74 and 0.59, respectively). It is evident that the different sensors can generate a relatively similar N rate application file if data are collected at the same time and if the same agronomic model is used. The advantage of the tractor sensor is that it can be used under different weather conditions, at any time of day (if active), and the whole process of scanning and application can be automated. Mapping and detailed positioning are not necessary in the real-time solution, making it simple to use in practice. However, an advantage of pre-fertilisation mapping with satellite or drone is that it provides an overview of the entire field, which can be useful in decision-making and the fertilisation strategy can be adapted accordingly. There are also economic differences between tools that can be decisive for users.

There are different approaches for transferring data from the real-time sensors to actuation, e.g. applying the right amount of N. In the simplest approach, the farmer scans a small reference area considered representative of the average N requirement. The system may then vary the N application through a built-in model (e.g. adding more N in areas with lower vegetation index values, with some restrictions as in the case in Fig. 8). Some systems allow the user to use two arbitrary reference areas (high, low) and distribute according to the difference. In these cases, the farmer may use expert knowledge to manually set a desired N rate. Various tools can be used to guide the farmer to a suitable N rate. Small on-farm experiments (Lacoste et al. 2022) such as zero-plots (no N added; example shown in Fig. 8) and/or max-plots or maxstrips (sufficient N applied to ensure N is not limiting for crop growth) can be used as reference in estimation of N rate (e.g. Johnson and Raun 2003; Lukina et al. 2001). Such plots are intended to indicate the level of soil N supply and yield potential, respectively, in the actual growing season (e.g. Raun et al. 2001). An approach that does not require a real max-plot is to use a so-called virtual reference plot (Holland and Schepers 2013), which takes e.g. the 95-percentile vegetation index value of the field as a max value. The information from such on-farm experiments can be used in the calculation of a suitable N rate to apply (Piikki et al. 2022).

5 Examples of handheld sensors and sensors in contact with plants

Some real-time sensor systems have the same components as some handheld spectrometers, such as the active sensors GreenSeeker (Trimble/Case, USA) and the RapidScan CS-45 (Holland Scientific, USA), which has similar optics to the OptRx tractor system. In addition, both passive and active versions of the Yara N-Sensor exist as handheld units. Such instruments are particularly useful in research, in small-plot field trials, and in evaluating on-farm experiments (e.g. producing data to be used in calibrations of real-time sensors). Handheld

hyperspectral sensors are also used in spectroscopic research, e.g. instruments such as ASD Fieldspec 4 (Malvern Panalytical, USA) can record reflectance in contiguous narrow bands from 350 to 2500 nm. Such instruments can be used in the development of new crop sensor applications (e.g. Pierna *et al.* 2022). Another type of handheld instrument uses ultraviolet fluorescence. One such instrument is the Multiplex (FORCE-A, France), which uses light-emitting diodes (in visible and ultraviolet (375 nm) light) and filtered photodiodes for screening of chlorophyll fluorescence (Ben Ghozlen *et al.* 2010). The instrument provides different fluorescence indices that have been shown to be useful for detecting nutrient stress, diseases and e.g. maturity and quality in grapes (Agati *et al.* 2018).

The now classical handheld absorbance-based SPAD meter was developed by Minolta (Konica Minolta, Japan) in the 1980s, although the development of such an instrument was described earlier (Wallihan 1973). The SPAD-502 meter indirectly measures the chlorophyll content per unit leaf area based on transmittance of red (650 nm) and infrared (940 nm) radiation through the leaf when a light source and a detector are clamped around a leaf. The Yara N-tester (Yara, Norway) is an adaptation of the SPAD meter with calibrations of N requirement for a range of crops. A non-linear relationship between SPAD meter readings, the Yara N-tester and chlorophyll concentration in different crops has been described by e.g. Uddling et al. (2007). To acquire representative readings for a crop stand, a number of measurements must be made on different leaves. For example, in small-grain cereals, measurement with the Yara N-tester should be made on 30 leaves (flag leaves) to get a reading. Other brands of chlorophyll meters using the same principle are now also available. The Dualex Scientific (FORCE-A, France) is a similar type of sensor, but it uses ultraviolet light to quantify chlorophyll concentration and polyphenol content. Chlorophyll meters have been shown to be useful for calibrating real-time sensors and other remote sensing data, since it is laborious to generate data with spatial coverage using chlorophyll meters alone (e.g. Miao et al. 2008; Söderström et al. 2017).

Since chlorophyll meters can give a quantitative measure of the N concentration in crop leaves (e.g. per unit fresh weight or leaf area), these instruments can also be used to measure N uptake (kg N ha $^{-1}$) when combined with information on biomass. In a pilot study, Blackert (2018) found that handheld GreenSeeker measurements and chlorophyll meter readings in combination were well correlated ($R^2 = 0.96$) with analysed N uptake (kg N ha $^{-1}$). A commercial service is now available (from Yara, Norway) in which the ground coverage of the crop based on an ordinary digital photo is combined with Yara N-tester readings to quickly assess N uptake.

High-throughput field phenotyping in plant breeding is a field of research that is related to precision agriculture, but the requirements differ due to

differences in scale, e.g. size and number of plots and fields. Sometimes even the detailed structure of individual plants can be of interest in this type of research. In a review by Chawade et al. (2019), a multitude of techniques were described. Some are similar to those used in practical precision agriculture and others have the potential to be included, e.g. as part of tractor-mounted real-time sensor solutions. Examples are different techniques to capture plant structure and crop height, which could be useful to further refine assessments of nutrient requirements and plant protection management. Such techniques involve the creation of point clouds that can be used to assess biomass and describe plant height, leaf area and leaf angle. Light detection and ranging (LiDAR) or, more simply, photogrammetric analysis of a series of overlapping photos (structure from motion, SfM) are examples of techniques used. An alternative approach for measuring crop height is to use ultrasonic sensors, which typically use time-of-flight of a reflected sound wave from a transmitter to a receiver. This type of technique has proven useful in practical solutions in geometric characterisation of crops and in nitrogen and water management (Bronson et al. 2021; Moreno and Andújar 2023).

6 Case Study 1: Comparison of sensors for prediction of N uptake in oats

6.1 Oats - an important crop

Around two-thirds of the world's oats (Avena sativa L.) are produced in Europe, Canada and Russia (USDA; https://apps.fas.usda.gov/psdonline, data from 2023), with reported global average yield of around 2.5 t ha⁻¹ but 2- to 3-fold higher yields in countries with more intense production. In Sweden, oats are the third largest cereal crop grown and in recent years new markets have developed, such as substitutes for rice and dairy products. With this increased importance, a better basis for fertiliser recommendations for oat crops is required. In Swedish spring oats, N is currently mainly applied at sowing, with an optional topdressing shortly after crop emergence. Based on previous Swedish experiments on oats, N fertiliser can be split into two doses, with the second applied at stem elongation (Zadoks' growth stage DC 32-37; Zadoks et al. 1973), without affecting yield compared with applying all N at sowing (e.g. Krijger 2011). One benefit of split fertiliser application is that it allows the fertiliser level to be adjusted at a stage when it is easier to predict soil N delivery during the growing season (Delin and Stenberg 2014; Walsh and Walsh 2020). Adjustment of N fertilisation to current crop status within and between fields using crop sensors has been successfully performed for other crops (Berger et al. 2020; Diacono et al. 2012; Mulla 2013).

6.2 Split N application can be beneficial

A recent study by Engström *et al.* (2024) investigated the effect of split N application on yield and quality in four spring oat varieties, with topdressing of N at DC 31 and DC 45, in three small-plot field experiments per year at different sites in south-west Sweden (Götala, Multorp, Lanna) in 2020, 2021 and 2022 (Fig. 9). The soil type is sandy loam at Götala, silty clay loam at Multorp and silty clay at Lanna. The sowing date was mainly around April 15, but varied from April 3 at Götala in 2020 to April 22 at Lanna in 2022. The preceding crop was winter wheat or spring oats at all sites and in all years. The results indicated that EONR for oats (kg ha⁻¹) could be explained by yield at EONR (OptN_{vield})

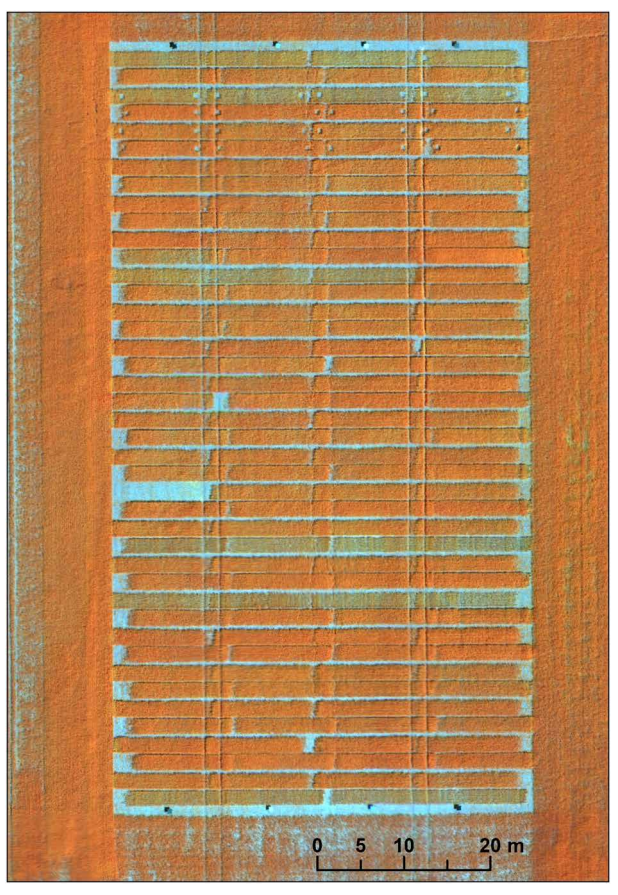


Figure 9 Design of one of the small-plot field experiments on oats in the case study. False-coloured image from the Micasense Rededge drone camera (red = NIR band; green = red band; blue = green band). Reflectance panels can been seen along the edges and marks after cutting the crop are visible in parcels in the upper part of the trial.

(t ha^{-1}) and N uptake (kg ha-1) in unfertilised plots at DC 31-32 (Eq. 3) and 43-47 (Eq. 4):

$$EONR = 93 + 11 \times OptN_{viold} - 1.7 \times N \text{ uptake}$$
 (Eq. 3)

$$EONR = 74 + 14 \times OptN_{vield} - 1.0 \times N \text{ uptake}$$
 (Eq. 4)

When determining EONR, the grain/fertiliser price ratio was in this case set to 8.0 (based on the average of the previous 10-year period) (Engström *et al.* 2024). Topdressing at the later stage (DC 43-47) increased the chances of higher protein and more accurate prior prediction of EONR ($R^2 = 0.96$ vs. 0.70 at DC 31-32). Another finding was that estimation of N uptake by a crop sensor during these growth stages would enable variable rate application.

In the case study, prediction models of N uptake were developed with four different multispectral crop sensors. To determine N uptake during the season, the crop was cut (2 × 0.25 m² areas) in each plot (total plot size ~2 m × 10 m) in N fertilisation treatments supplying 0, 70, 100 and 160 kg N ha⁻¹, for all varieties in one block and on two occasions, DC 31-32 and DC 43-47. Crop samples were dried at maximum 55°C, N concentration was analysed and N uptake was calculated. On the same occasions in each plot, before cutting, measurements of crop canopy reflectance were carried out with two handheld spectrometers and two drone-borne multispectral cameras. The handheld sensors were Yara N-Sensor ALS (Yara, Norway) and RapidScan-CS-45 (Holland Scientific, USA), although the RapidScan sensor was only used in two seasons (2021 and 2022). The drone cameras were a five-band Micasense Rededge camera (AgEagle, USA; with similar bands as Micasense Altum in Fig. 4) and a nine-band MAIA camera (Eoptis Srl., Italy; with bands the same as Sentinel-2 in Fig. 4).

The measurements with these sensors were made in a manner commonly applied or recommended by the instrument provider. With the handheld Yara N-Sensor, the value recorded for each parcel was the average of four measurements made from each parcel corner from about 1.5 m above the ground, at an angle of about 45°. With the RapidScan, continuous scanning and logging of data were carried out while walking along one side of each parcel (holding the instrument 0.5–1.0 m above the canopy, at an angle of 45° so that the instrument was aimed at the centre of the parcel). The drone cameras were mounted on the same drone (a customised Explorian-8, Pitchup, Sweden). The flights were carried out with a sun angle of not less than 45°, each flight in as uniform weather as possible (either sunny or cloudy). Flight altitude was 80 m and flight speed 5 m s^{-1} . The image overlap was at least 80%. Both cameras had an incoming light sensor, from which data were used in image post-processing. The Micasense Rededge was calibrated with a photo of the target panel before and after each flight, whereas for the MAIA camera 50 cm × 50 cm reflectance panels (from MosaicMill Oy, Finland) were used, with reflectance 2%, 8%, 23%

and 44% (in all bands). Image mosaics were made with the Solvi web service (Solvi AB, Sweden; https://solvi.ag). The reflectance panels were placed within the field trial (as seen in Fig. 9) and used to establish a relationship between digital numbers in the different bands and the values of the panels. Calibration of the mosaics was then done using this empirical relationship ('empirical line method'; Aasen et al. 2018).

The average reflectance values for each parcel and for each sensor were extracted and compared with the results of laboratory analyses on the cut plant samples. A range of different vegetation indices were computed and comparisons were made through bivariate and multivariate regression analyses. Prediction models were validated through a leave-one-trial-out procedure and also a leave-one-year-out procedure. Results of the leave-one-year-out evaluation and results obtained using the generally best-performing bivariate linear or non-linear model between sensor data and reflectance data are reported here.

The best-performing individual vegetation index in this case was chlorophyll index (ChlI) (Gitelson *et al.* 2003), although the difference compared with some other similar red edge indices, such as NDRE, was very small. The chlorophyll index is simply based on the ratio of two bands (ρ) in the red edge-NIR region:

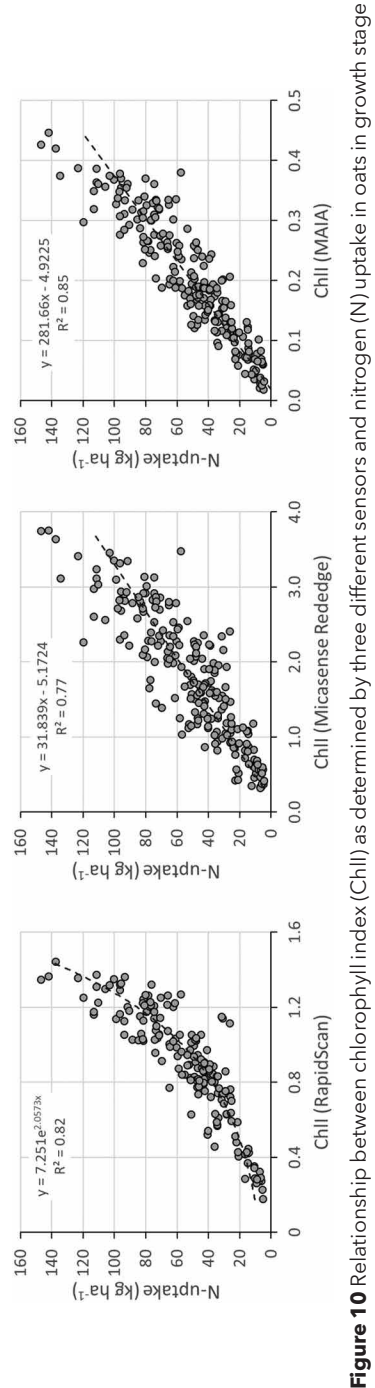
$$ChII = (\rho_{NIR}/\rho_{Red edge}) - 1$$
 (Eq. 5)

For the Yara N-Sensor, only the internal vegetation index (Sl_{Yara}) was used, details of which are not publicly available. The Sl_{Yara} values obtained have been shown to be strongly correlated with ChII (e.g. Söderström et al. 2017). For the RapidScan sensor, the bands NIR (780 nm) and RE (730 nm) were used for calculation of ChII. For Micasense Rededge, camera bands 5 (840 nm) and 4 (717 nm) were used, while for the MAIA device sensor bands 7 (783 nm) and 6 (740 nm) were used.

6.3 Predicting N uptake in oats with crop sensors

Overall in the experiments, N uptake (kg N ha⁻¹) was very similar in 2021 (mean = 58, σ = 28, n = 96) and 2022 (mean = 52, σ = 32, n = 96), but lower in 2020 (mean = 28, σ = 23, n = 32). For all sensors, there was a relatively strong correlation between the vegetation index and analysed N uptake. The relationship was linear in all cases except for the RapidScan sensor, where the data followed an exponential function (Fig. 10). Since the different crop sensors used record reflectance in different bands, the calculated ChII was expected to differ.

As can be seen in Fig. 10, the Chll values differed substantially between the sensors. For the RapidScan (left panel in Fig. 10), there was an exponential



DC 31-47 determined in the laboratory. Diagram based on data from 2 years for the RapidScan sensor, and on data from 3 years for the other sensors.

relationship between ChlI index and crop N uptake. For the drone cameras (centre and right panels), only a few very high N uptake values (>100–120 kg N ha⁻¹) tended to deviate from a linear relationship. The reason for the exponential behaviour of data from the RapidScan sensor is uncertain. Measurements with that instrument were made at an angle, so more of the plant affected the data. However, this was also the case with the Yara N-Sensor, although that instrument uses an internal vegetation index. Making measurements at an angle could be an advantage e.g. if the crop stand is thin, by reducing the impact of soil. Moreover, RapidScan is an active sensor and some studies suggest that these may be more strongly affected by the uppermost part of the plant stand compared with passive sensors (Winterhalter *et al.* 2013). Therefore even though the bands in RapidScan are relatively similar to the bands used in the MAIA camera, differences in the instrument and in the measurement procedure can cause differences in the values produced.

Results of the leave-one-year-out validation are displayed in Table 1. This type of challenging validation should indicate the general performance of prediction models, which is useful in assessment of use of the models in other locations and years. All sensors performed well ($R^2 > 0.7$, root mean square error of predictions (RMSEP) <20 kg N ha⁻¹). The nine-band drone camera (MAIA) had slightly higher R^2 value and the lowest prediction error of all sensors ($R^2 = 0.85$; RMSEP = 12 kg N ha⁻¹). Very high values of N uptake in a dense crop stand are most challenging to predict with sensors based solely on crop canopy reflectance. As mentioned earlier in this chapter, using information on crop height or structure of plants within the stand could possibly improve the model (e.g. Moreno and Andújar 2023). Combining information from different types of sensors may further improve predictions of N uptake.

Since all four sensors types performed relatively well at estimating N uptake up to about 100 kg ha⁻¹, they and other similar sensors could be useful tools for predicting EONR during the growing season, e.g. using the equations reported above (Eqs. 4 and 5). The choice of tool used depends on the type/s available for the farmer/advisor and how quickly and easily the

			· · · · · · · · · · · · · · · · · · ·			
	Years	Index	Type of model	R^2	RMSEP	
RapidScan	2021, 2022	Chll	Exponential	0.77	15 kg N ha ⁻¹	
Yara N-Sensor	2020–2022	SI_{Yara}	Linear	0.79	14	
Micasense Rededge	2020–2022	Chll	Linear	0.80	16	
MAIA	2020–2022	Chll	Linear	0.85	12	

Table 1 Results from leave-one-year-out validation of oats N uptake prediction models.

RMSEP = root mean square error of predictions vs. observed values. SI_{Yara} is the proprietary index of the Yara N-Sensor.

sensor data can be retrieved. The most challenging part in predicting EONR early in the season is accurate assessment of future yield, which is used in the calculation.

7 Case Study 2: Evaluation and upscaling of portable tools for crude protein determination and field mapping in conjunction with Sentinel-2 satellite imagery

7.1 Mapping of protein needed in nitrogen use efficiency estimations

This case study demonstrates how a portable NIR protein content analyser can be combined with satellite imagery and used to create field-scale crop protein maps. The study was conducted in two cropping seasons, 2021 and 2022, but the information presented here is a subset of the data, collected in 2022. An initial report on the study can be found in Morandin Figueiredo *et al.* (2023).

Ability to determine crop quality parameters in the field would greatly increase the capacity of growers to estimate the use efficiency of inputs, such as irrigation, fertilisation and plant protection products, allowing for more precise field management. Crude protein (CP) is an essential variable in terms of N use efficiency evaluations. In precision agriculture, it is currently relatively easy to keep track of applied rates of N fertiliser and of yield, but it is less common to have detailed knowledge about the protein concentrations in different parts of the field. A study by Börjesson *et al.* (2019) showed that CP in winter wheat could be predicted with mean absolute error (MAE) <1% by combining an early (end of stem elongation) and a late (milk development) satellite image. In a review of CP predictions, Bastos *et al.* (2021) noted that on-combine protein measurements are generally more accurate than CP predictions made using proximal or remote sensing. However, on-combine protein mapping is still very uncommon in practice.

An alternative procedure for CP mapping could be to combine a proximal CP sensor, to achieve a sufficient amount of ground observations, with remote sensing data from satellites or drones to generate within-field protein maps. One tool that can make this possible is the GrainSense (GS) Analyzer (GrainSense Oy, Finland). It employs NIR analysis methodology for grain CP determination by a portable handheld device with a built-in calibration model. The objective of this experiment was to evaluate the accuracy of this instrument in CP determination compared with the reference laboratory method and, if necessary, to test different calibration approaches and assess whether the data obtained from such tools can be used in combination with satellite imagery in a cost-effective alternative to protein mapping devices mounted on combine harvesters.

7.2 Methods and data

Winter wheat samples were harvested from producers' fields located within a $20 \text{ km} \times 20 \text{ km}$ area in south-west Sweden. A total of 46 samples were collected from five different fields with three different cultivars (two fields with cv. Reform, two fields with cv. Brons, one field with cv. Norin) during the 2022 cropping season. Each sample comprised nine subsamples collected in a 3-m radius using a Minibatt (Godé, France) electric handheld sample harvester. Samples were georeferenced using a Nomad handheld GNSS computer (Trimble, USA), to enable extraction of corresponding reflectance values from satellite images. The winter wheat samples were oven-dried at 40°C for 24 h and cleaned using a sample cleaner model MLN (Pfeuffer, Germany), before being submitted for analysis. Grain CP was determined by calculating the average of five subsamples using the GS tool. Reference CP value was obtained from laboratory analysis using an InfratecTM 1241 (Foss, Denmark) grain analyser, which uses near-infrared transmittance (NIT) methodology.

Statistical analyses were performed with R Statistical software (R Core Team 2022). The metrics used for evaluation of the models were Nash-Sutcliffe model efficiency (E), which measures how well predicted versus observed data fit the 1:1 line (Nash and Sutcliffe, 1970), MAE, which is the mean of the absolute difference between predicted and observed data, and coefficient of determination of a linear regression model between predicted and observed data (R^2).

Satellite images were obtained from the Sentinel-2 satellite Multi Spectral Instrument (MSI). Level-2A data (bottom of the atmosphere or surface reflectance; Obregón et al. 2019) were extracted for each sample point from the images in ArcGIS Pro, version 2.5.1 (ESRI 2023). Among the bands available from the satellite MSI, only nine bands were used: bands 02 (490 nm), 03 (560 nm), 04 (665 nm), 05 (705 nm), 06 (740 nm), 07 (783 nm), 8A (865 nm), 11 (1610 nm) and 12 (2190 nm). Output images from the Level-2A processing at 20 m spatial resolution contain all bands available from the satellite MSI and therefore 20 m was chosen as the resolution for the present work. Images were gathered from late May, which corresponds to flag leaf emergence in winter wheat (Zadoks' growth stage DC 37) and is when farmers in Sweden usually apply topdressing fertiliser, to late July, which is close to maturity (>DC 80). The images were screened and images with clouds covering any portion of the included fields in the study were discarded. Only five images in the date range were considered suitable for analysis in 2022 (Table 2).

Table 2 Satellite image dates used for analysis.

Year	Image dates (DD/MM)
2022	29/05, 05/06, 25/06, 30/06, 15/07

7.3 Calibrating the GrainSense instrument

There was a significant difference between GS and laboratory reference values, making it necessary to develop instrument calibration models prior to using the data from the GS tool in the upscaled modelling. Models to correct the protein content from the GS tool were built by linear regression, using the GS data as predictor variables and the laboratory data as response variables. Two approaches were evaluated: general calibration, where the entire dataset was used to parameterise the model, and field-specific calibration, where the dataset was split and field-specific models were built. Overall, field-specific calibration models outperformed the general model, with MAE ranging from 0.14% to 0.26%, compared with 0.38% for the general model (Table 3 and Fig. 11). The final model for the Bjertorp West site had very low MAE,

Table 3 Nash-Sutcliffe model efficiency (E), mean absolute error (MAE) and coefficient of determination of linear regression models (R^2) for field-specific and general calibration models for crude protein (CP) prediction in winter wheat.

					Mean CP (%)	
Field	Cultivar	E	MAE (%)	R^2	Observed	Predicted
Bjertorp West	Brons	-0.09	0.14	0.11	10.68	10.69
Bjertorp North	Norin	0.85	0.17	0.86	11.58	11.56
Kilagarden North	Reform	0.94	0.26	0.94	12.36	12.36
Skofteby Northeast	Brons	0.87	0.23	0.87	11.67	11.65
Skofteby Southeast	Reform	0.97	0.20	0.97	11.57	11.58
General model		0.83	0.38	0.83	11.57	11.57

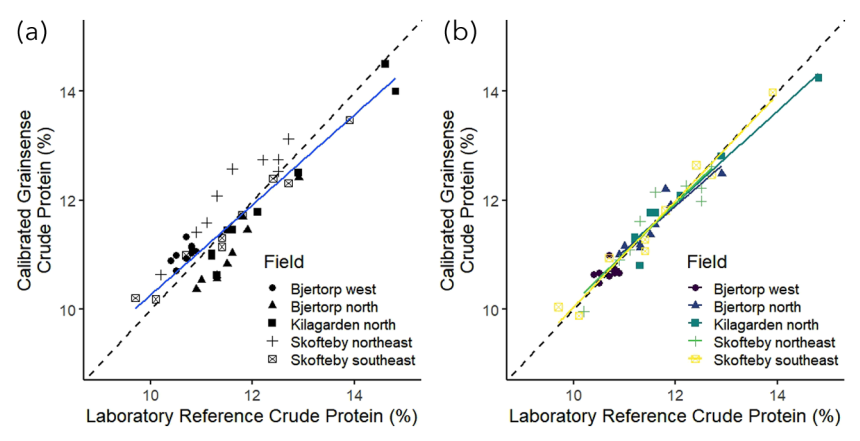


Figure 11 Results of leave-one-out cross-validation of (a) general and (b) field-specific calibration models for GrainSense crude protein analysis. Dashed lines represent the 1:1 ratio.

but the model was not robust due the fact that the data used to build it had a very small range.

7.4 Combining proximal and remote sensing to produce protein maps for wheat

Grain CP prediction models were built by linear regression and the same approach as used for the calibration models was followed. General and field-specific prediction models were developed with the objective of upscaling the GS data in combination with satellite data to generate CP field maps. Calibrated GS data were used as response variables and reflectance data from the satellite images as predictor variables in different configurations. Individual bands (ρ) and combinations of two, three and four bands were tested. Normalised difference indices, NDI_{i,j} = ([$\rho_i - \rho_j$] / [$\rho_i + \rho_j$]), were also calculated using all combinations of two individual bands and were evaluated individually and in two, three and four index combinations. The models were tested for every available image, individually and in two and three image sequences. For the image sequences, the same bands or indices per image were used. The total number of models evaluated is shown in Table 4. Final selection was based on the lowest MAE for both general and field-specific models.

The predictor variables for the selected models varied for each field-specific and general models, as shown in Table 5The best predictors included combinations of two indices from two images.

Grain CP prediction models followed the same trend as the calibrations, with field-specific models outperforming the general models (Fig. 12).

Table 4 Wheat grain crude protein (CP) regression combinations tested using nine different bands in 20-m spatial resolution images from the Sentinel-2 satellite.

Predictor variables	Number of combinations		
Single band	45		
Single band, 2 image sequence	90		
Single band, 3 image sequence	90		
2/3/4 band combinations	180/420/630		
2/3/4 band combinations, 2 image sequence	360/840/1260		
2/3/4 band combinations, 3 image sequence	360/840/1260		
Vegetation indices	180		
Vegetation indices, 2 image sequence	360		
Vegetation indices, 3 image sequence	360		
Vegetation index combinations	3150		
Vegetation index combinations, 2 image sequence	6300		
Vegetation index combinations, 3 image sequence	6300		

11.56

specific and general models for crude protein (CP) prediction in winter wheat.					
				Mean CP (%)	
Field	Е	MAE (%)	R^2	Observed	Predicted
Bjertorp West ^a	-0.11	0.14	0.11	10.68	10.69
Bjertorp North ^b	0.85	0.17	0.85	11.58	11.56
Kilagarden North ^c	0.94	0.27	0.94	12.36	12.36
Skofteby Northeast ^d	0.87	0.22	0.87	11.67	11.66
Skofteby Southeast ^e	0.96	0.22	0.96	11.57	11.56

0.74

11.57

0.45

Table 5 Nash-Sutcliffe model efficiency (E), mean absolute error (MAE), coefficient of determination of linear regression models (R^2) and final model predictor variables for field-specific and general models for crude protein (CP) prediction in winter wheat.

0.73

General modelf

 $f_{P_{3'}}$, $P_{7'}$, P_{8A} and P_{12} from image 29/05, 05/06 and 15/07.

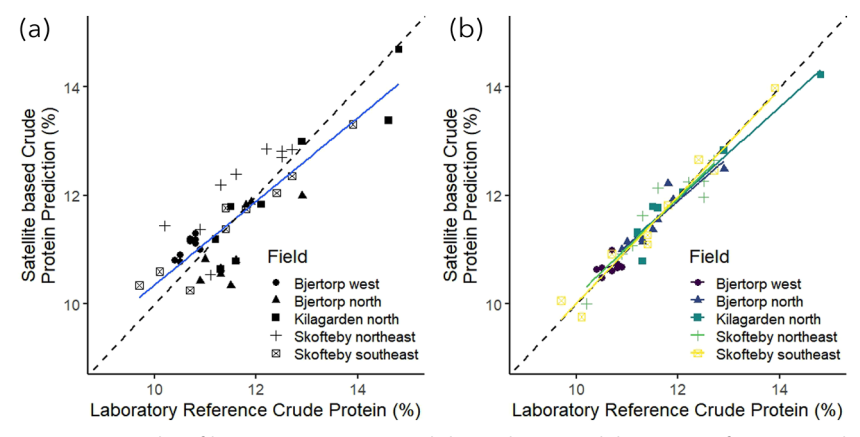


Figure 12 Results of leave-one-out cross-validation between laboratory reference crude protein (CP) and predicted CP from selected (a) general and (b) field-specific prediction models. Dashed lines represent the 1:1 ratio.

Variability in yearly weather conditions, cultivar releases and management practices make it necessary to update prediction models on a seasonal basis to reflect current conditions. An approach was proposed comprising four simple steps that farmers can deploy to obtain grain CP maps:

- Take a number of grain samples from each field.
- Determine CP in all samples using the GS sensor and send part of the samples for laboratory analysis of CP.

 $^{^{\}rm a}{\rm NDI}_{\rm 2,7}$ and ${\rm NDI}_{\rm 6,12}$ from images 29/05, 05/06 and 15/07.

^bNDI_{3,4} and NDI_{4,11} from images 29/05, 25/06 and 15/07.

 $^{^{}c}\rho_{6}$ and ρ_{12} from images 29/05, 05/06 and 15/07.

 $^{^{}d}\rho_{6}$ and ρ_{12} from images 25/06, 30/06 and 15/07.

 $^{{}^{\}circ}NDI_{2,12}$ and $NDI_{3,12}$ from images 05/06, 25/06 and 15/07.

- Calibrate a model for correction of sensor-based CP values (preferably per field) and apply that on non-laboratory analysed samples.
- Use the corrected CP values to calibrate a satellite-based model for CP mapping.

In a decision support system, the procedure could be simplified for the user and all combinations of bands and image dates could be automatically tested to find the best model for CP mapping. Field-specific models generally outperform general models. A dynamic system which selects the best predictors based on the conditions of the current crop could account for variations across fields due to soil properties and management practices. In addition, continuous in-season reflectance measurements could be used to account for variations in crop growth due to different cultivars and environmental conditions.

Small and relatively simple-to-use proximal sensors, such as the GS tool, have great potential as a cost-effective, fast and accurate method for grain CP analysis, although they rely on either the manufacturer or the end-user to develop calibration curves. If used in conjunction with the proposed satellite-based system, it would be possible to upscale local CP predictions to highly accurate CP field maps that can be combined with yield maps and nitrogen (N) input to generate N use efficiency maps. It is interesting to note that in all fields, the best combination of vegetation indices for predicting CP included bands in the SWIR region (Table 5; SWIR region shown in Fig. 3). As mentioned, the sensors currently employed in precision agriculture applications most commonly use bands in the vis-NIR region of the electromagnetic spectrum (examples shown in Fig. 4). This case study shows the usefulness also of bands in the SWIR region.

8 Outlook and Conclusion

A recent report described 'plant wearables' as technology with the potential to revolutionise plant production (World Economic Forum 2023). These can be miniature, low-cost, even biodegradable sensors that are attached e.g. on leaves for monitoring variables such as temperature, humidity, moisture and nutrient levels. Through continuous logging and transmission of data, such sensors, as part of the Internet-of-Things, could facilitate real-time surveillance of detailed plant health and field conditions. More efficient data sharing and integration of data from different sources, including plant wearables, can be expected to contribute to better decision support and more precise use of precision agriculture technologies. Some techniques described in this chapter, such as camera-assisted SSWM and sensor-based N application, could benefit from additional information, e.g. on soil properties and yield potential. The ongoing digitisation of agriculture and the explosion of applications using

artificial intelligence are likely to affect crop production and agricultural advisory and support services in unforeseen ways in the near future. In combination with new methods and other available sensing techniques, proximal crop sensing will likely be used even more commonly in future, as part of efforts to meet local and global challenges.

9 Where to look for further information

This text does not completely cover the field of proximal crop sensors. Other sensors, techniques and applications exist. To get more in-depth details, a good approach can be to read a textbook such as Heege (2013), which does provide a broad coverage of precision farming principles, and a few review articles, e.g. Chawade et al. (2019), Gerhards et al. (2022) and Lo Presti et al. (2023).

In addition, members of the International Society of Precision Agriculture (https://ispag.org) have access to a goldmine of information through all articles in the journal Precision Agriculture, and the comprehensive ICPA and ECPA conference proceedings.

10 References

- Aasen, H., Honkavaara, E., Lucieer, A., and Zarco-Tejada, P.J. 2018. Quantitative remote sensing at ultra-high resolution with UAV spectroscopy: a review of sensor technology, measurement procedures, and data correction workflows. *Remote Sensing* 10, 1091. https://doi.org/10.3390/rs10071091
- Adamchuk, V., Ji, W., Viscarra Rossel, R., Gebbers, R., Tremblay, N. 2018. Chapter 9. Proximal soil and plant sensing. In Shannon, D. K., Clay, D. E., Kitchen, and N. R. (Eds.). *Precision Agriculture Basics*. ASA, CSSA, and SSSA Books. Madison, WI, USA; pp. 123–145. https://doi.org/10.2134/precisionagbasics
- Agati, G., Soudani, K., Tuccio, L., Fierini, E., Ben Ghozlen, N., Mostafa Fadaili, E., et al. 2018. Management zone delineation for winegrape selective harvesting based on fluorescence-sensor mapping of grape skin anthocyanins. *Journal of Agricultural and Food Chemistry* 66, 5778–5789. https://doi.org/10.1021/acs.jafc.8b01326
- Allmendinger, A. Spaeth, M., Saile, M., Peteinatos, G.G., and Gerhards, R. 2022. Precision chemical weed management strategies: a review and a design of a new CNN-based modular spot sprayer. *Agronomy* 12, 1620. https://doi.org/10.3390/agronomy12071620
- Bastos, M., de Borja Reis, F., Sharda, A., Wright, A., and Ciampitti, I.A. 2021. Current status and future opportunities for grain protein prediction using On-and Off-combine sensors: a synthesis-analysis of the literature. *Remote Sensing* 13, 5027. https://doi.org/10.3390/rs13245027
- Ben Ghozlen, N., Cerovic, Z.G., Germain, C., Toutain, S., and Latouche, G. 2010. Nondestructive optical monitoring of grape maturation by proximal sensing. *Sensors* 10, 10040–10068. https://doi.org/10.3390/s101110040

- Berger, K., Verrelst, J., Féret, J., Wang, Z., Wocher, M., Strathmann, M., et al. 2020. Crop nitrogen monitoring: recent progress and principal developments in the context of imaging spectroscopy missions. *Remote Sensing of Environment* 242, 111758.
- Blackert, C. 2018. Kväveupptag i höstvete med Blackert-metoden (Nitrogen uptake in winter wheat using the Blackert method), *Arvensis* 7, 12–14. Retrieved 28/01/2024 from https://pos.agrovast.se/wp-content/uploads/sites/5/2019/01/2370.pdf
- Börjesson, T., Wolters, S., and Söderström, M. 2019. Satellite-based modelling of protein content in winter wheat and malting barley. In Stafford J.V. (Ed.). Precision Agriculture 19, Proceedings of the 12th European Conference on Precision Agriculture, Wageningen Academic Publishers, Wageningen, The Netherlands, pp. 581–587.
- Brodt, S., Six, J., Feenstra, G., Ingels, C., and Campbell, D. 2011. Sustainable agriculture. *Nature Education Knowledge* 3(10), 1.
- Bronson, K.F., French, A.N., Conley, M.M., and Barnes, E.M. 2021. Use of an ultrasonic sensor for plant height estimation in irrigated cotton. *Agronomy Journal* 113, 2175–2183. https://doi.org/10.1002/agj2.20552
- Chawade, A., van Ham, J., Blomquist, H., Bagge, O., Alexandersson, E., and Ortiz, R. 2019. High-throughput field-phenotyping tools for plant breeding and precision agriculture. *Agronomy* 9, 258. https://doi.org/10.3390/agronomy9050258
- Delin, S., and Stenberg, M. 2014. Effect of nitrogen fertilization on nitrate leaching in relation to grain yield response on loamy sand in Sweden. *European Journal of Agronomy* 52, 291–296.
- Diacono, M., Rubino, P., and Montemurro, F. 2012. Precision nitrogen management of wheat: a review. *Agronomy for Sustainable Development* 33, 219–241.
- Engström, L., Delin, S., Wetterlind, J., Jonsson, A., and Syed Rehmat Ullah, S. 2024. Optimum N-rate and effect of split N fertilization timing on yield and quality in spring oat varieties. Submitted to Agricultural and Food Science 33, 164–174. https://doi.org/10.23986/afsci.143565
- ESRI Inc. 2023. ArcGIS Pro (Version 2.5.1). ESRI Inc. Retrieved 28/03/2024 from https://www.esri.com/en-us/arcgis/products/arcgis-pro/overview
- European Parliament. 2019. Precision agriculture and the future of farming in Europe: scientific foresight study. https://doi.org/10.2861/175493
- Gerhards, R., Andújar Sanchez, D., Hamouz, P., Peteinatos, G.G., Christensen, S., and Fernandez-Quintanilla, C. 2022. Advances in site-specific weed management in agriculture–a review. *Weed Research* 62, 123–133. https://doi.org/10.1111/wre.12526
- Gitelson, A.A., Gritz, Y., and Merzlyak, M.N. 2003. Relationships between leaf chlorophyll content and spectral reflectance and algorithms for non-destructive chlorophyll assessment in higher plant leaves. *Journal of Plant Physiology* 160, 271–282.
- Heege, H.J. 2013. Precision in Crop Farming. Site Specific Concepts and Sensing Methods: Applications and Results. Springer, Dordrecht, The Netherlands, 356 p. https://doi.org/10.1007/978-94-007-6760-7
- Holland, K.H., Schepers, J.S. 2013. Use of a virtual-reference concept to interpret active crop canopy sensor data. *Precision Agriculture* 14, 71–85. https://doi.org/10.1007/s11119-012-9301-6
- Hu, K., Wang, Z., Coleman, G., Bender, A., Yao, T., Zeng, S., Song, D., Schumann, A., and Walsh, M., 2024. Deep learning techniques for in-crop weed recognition in

- large-scale grain production systems: a review. *Precision Agriculture* 25, 1–29. https://doi.org/10.1007/s11119-023-10073-1
- Johnson, G.V., and Raun, W.R. 2003. Nitrogen response index as a guide to fertilizer management. *Journal of Plant Nutrition* 26, 249–262. https://doi.org/10.1081/PLN -120017134
- Karlsson Potter, H., Delin, S., Engström, L., Stenberg, B., and Hansson, P.-A. 2022. Precision nitrogen application – potential to lower the climate impact of crop production. *Mistra Food Futures Report 9*, Swedish University of Agricultural Sciences, Uppsala, Sweden, 37 p. Retrieved 28/03/2024 from https://mistrafoodfutures.se/wp-content/ uploads/2022/11/mistra-food-futures-report-9-web.pdf
- Kindred, D.R., Hatley, D., Ginsburg, D., Catalayud, A., Storer, K., Wilson, L., et al. 2016. Automating Nitrogen Fertiliser Management for Cereals (Auto-N). AHDB Project Report No.561. Agriculture and Horticulture Development Board. Rothamsted Research, Harpinden, UK. Retrieved 28/03/2024 from https://repository.rothamsted.ac.uk/item/96x66/automating-nitrogen-fertiliser-management-for-cereals-auto-n-ahdb-project-report-no-561
- Krijger, A.-K. 2011. Kvävegödsling till havre. Mellansvenska försöksrapporten 2010 (Nitrogen fertilisation in oats. Mid-Swedish trials' report 2010), pp. 49–52. Retrieved 28/03/2024 from https://www.ffe.slu.se/Webdata/\$serie/03F5R2010Kvaeve goedsling_till_havre.pdf
- Lacoste, M., Cook, S., McNee, M., Gale, D., Ingram, J., Bellon-Maurel, V., et al. 2022. On-farm experimentation to transform global agriculture. *Nature Food* 3, 11–18. https://doi.org/10.1038/s43016-021-00424-4
- Lo Presti, D., Di Tocco, J., Massaroni, C., Cimini, S., De Gara, L., Singh, S., et al. 2023. Current understanding, challenges and perspective on portable systems applied to plant monitoring and precision agriculture. *Biosensors and Bioelectronics* 222, 115005. https://doi.org/10.1016/j.bios.2022.115005
- Lukina, E.V., Freeman, K.W., Wynn, K.J. Thomason, W.E., Mullen, R.W., Klatt, A.R., et al. 2001. Nitrogen fertilization optimization algorithm based on in-season estimates of yield and plant nitrogen uptake. *Journal of Plant Nutrition* 24, 885–898.
- Miao, Y., Mulla, D.J., Randall, G.W., Vetsch, J.A., and Vintilla, R. 2008. Combining chlorophyll meter readings and high spatial resolution remote sensing images for in-season site-specific nitrogen management of corn. *Precision Agriculture* 10, 45–62. https://doi.org/10.1007/s11119-008-9091-z
- Morandin Figueiredo, B., Söderström, M., Persson, K., and Börjesson, T. 2023. Evaluation of portable tools for fast field assessment of winter wheat grain quality. In Stafford, J.V. (Ed.). *Precision Agriculture 23. Proceedings of the 14th European Conference on Precision Agriculture*, Wageningen Academic Publishers, Wageningen, The Netherlands, pp. 145–151. https://doi.org/10.3920/978-90-8686-947-3_16
- Moreno, H., Andújar, D. 2023. Proximal sensing for geometric characterization of vines: a review of the latest advances. *Computers and Electronics in Agriculture* 210, 107901.
- Mulla, D.J. 2013. Twenty five years of remote sensing in precision agriculture: key advances and remaining knowledge gaps. *Biosystems Engineering* 114, 358–371.
- Nash, J.E., and Sutcliffe, J.V. 1970. River flow forecasting through conceptual models part I–a discussion of principles. *Journal of Hydrology* 10, 282–290.
- Nilsson, M., Ardö, J., Söderström, M. Allard, A., Brown, A., and Webber, L. 2023. Remote sensing and Earth observation systems. In Allard, A. et al. (Eds.). *Monitoring*

- Biodiversity. Combing Environmental and Social Data. Routledge, Taylor & Francis Group, London and New York, pp. 122–147. https://doi.org/10.4324/9781003179245
- Obregón, M.Á., Rodrigues, G., Costa, M. J., Potes, M., and Silva, A.M. 2019. Validation of ESA sentinel-2 L2A aerosol optical thickness and columnar water vapour during 2017–2018. *Remote Sensing* 11, 1649.
- Pierna, J.A.F., Vermeulen, P., Chamberland, N., Decruyenaere, V., Froidmont, E., Minet, O., et al. 2022. Performance of three handheld NIR spectrometers for predicting grass silage quality. *Biotechnology, Agronomy, Society and Environment* 26, 309–318. https://doi.org/10.25518/1780-4507.19918
- Piikki, P., Söderström, M., and Stadig, H. 2022. Remote sensing and on-farm experiments for determining in-season nitrogen rates in winter wheat options for implementation, model accuracy and remaining challenges. *Field Crops Research* 289, 108742. https://doi.org/10.1016/j.fcr.2022.108742
- Rasmussen, J., Nielsen, J., Garcia-Ruiz, F., Christensen, S., and Streibig, J.C. 2013. Potential uses of small Unmanned Aircraft Systems (UAS) in weed research. *Weed Research* 53, 242–248.
- R Core Team. 2022. R: A Language and Environment for Statistical Computing. R Foundation for Statistical Computing, Vienna, Austria. https://www.R-project.org/
- Raun, W.R., and Johnson, G.V. 1999. Improving nitrogen use efficiency for cereal production. *Agronomy Journal* 91, 357–363. https://doi.org/10.2134/agronj1999.00021962009100030001x
- Raun, W.R., Solie, J.B., Johnson, G.V., Stone, M.L., Lukina, E.V., Thomason, W.E., et al. 2001. In-season prediction of potential grain yield in winter wheat using canopy reflectance. Agronomy Journal 93, 131–138. https://doi.org/10.2134/agronj2001 .931131x
- Reusch, S. 2005. Optimum waveband selection for determining the nitrogen uptake in winter wheat by active remote sensing. In Stafford, J. V. and Werner, A. (Eds.). Precision Agriculture '05. Proceedings of the 4th European Conference on Precision Agriculture, Wageningen Academic Publishers, Wageningen, The Netherlands, pp. 261–266.
- Reusch, S. 2006. N-sensor ALS® Basics, application and use. Landtechnik 61, 76–77.
- Söderström, M., Piikki, K., Stenberg, M, Stadig, H., and Martinsson, J. 2017. Predicting nitrogen uptake in winter wheat by combining proximal crop measurements with Sentinel-2 and DMC satellite images in a decision support system for farmers. *ACTA Agriculturae Scandinavica. Section B, Soil and Plant Sciences* 67, 637–650.
- Uddling, J., Gelang-Alfredsson, J., Piikki, K., and Pleijel, H. 2007. Evaluating the relationship between leaf chlorophyll concentration and SPAD-502 chlorophyll meter readings. *Photosynthesis Research* 91, 37–46. https://doi.org/10.1007/s11120-006-9077-5
- Wallihan, E.F. 1973. Portable reflectance meter for estimating chlorophyll concentrations in leaves. *Agronomy Journal* 65, 659–662. https://doi.org/10.2134/agronj1973.000 21962006500040039x
- Walsh, O.S., and Walsh, W.L. 2020. Nitrogen fertilizer rate and time effect on dryland no-till hard red spring wheat production. *Agrosystems, Geosciences & Environment* 3, 1–15. https://doi.org/10.1002/agg2.20093
- Winterhalter, L., Mistele, B., and Schmidhalter, U. 2013. Evaluation of active and passive sensor systems in the field to phenotype maize hybrids with high-throughput. *Field Crops Research* 154, 236–245.

- Wolters, S., Söderström, M., Piikki, K., Reese, H., and Stenberg, M. 2021. Upscaling proximal sensor N-uptake predictions in winter wheat (*Triticum aestivum* L.) with Sentinel-2 satellite data for use in a decision support system. *Precision Agriculture* 22, 1263–1283.
- World Economic Forum. 2023. Top 10 Emerging Technologies of 2023. Flagship report June 2023. Retrieved 28/01/2024 from https://www.weforum.org/publications/top-10-emerging-technologies-of-2023/
- Zadoks, J.C., Chang, T.T., and Konzak, C.F. 1974. A decimal code for the growth stages of cereals. *Weed Research* 14, 415–421. https://doi.org/10.1111/j.1365-3180.1974.tb01084.x